International Journal of Thermodynamics (IJoT)
ISSN 1301-9724 / e-ISSN 2146-1511
https://dergipark.org.tr/en/pub/ijot

Vol. 27 (No. 3), pp. 026-036, 2024
doi: 10.5541/ijot.145513
Published online: September 1, 2024

Research Article

Experimental and Numerical Investigation of Roughness Structure in Wind Turbine Airfoil at Low Reynolds Number

[1*]H. E. Tanürün, [2]A. G. Akın, [3]A. Acır, [4]İ. Şahin

[1]Kahramanmaraş Istiklal University, Elbistan Engineering Faculty, Department of Energy Systems Engineering, Kahramanmaraş, Türkiye
[2]T.C. Presidency of Defense Industries, Naval Platforms Department, Ankara, Turkey
[3]Gazi University, Faculty of Technology, Department of Energy Systems Engineering, Ankara, Turkey
[4] Purdue University, School of Mechanical Engineering, West Lafayette, 47906, USA
E-mail: [1]*erdi.tanurun@istiklal.edu.tr

Received 21 Mar. 2024, Revised 15 May 2024, Accepted 7 July 2024

Abstract

This paper experimentally and numerically investigates the effects of suction side surface roughness on the aerodynamic performances of the NACA 0015 turbine blade profile. Three different NACA 0015 turbine blade configurations, which are smooth (K_0), single roughness (K_1), and double roughness (K_2), are considered. The experimental studies were conducted using the HM-170 GUNT open wind tunnel model. The aerodynamic characteristics of these three blade configurations are evaluated in terms of their lift coefficient (C_L), drag coefficient (C_D), and aerodynamic efficiency (C_L/C_D). The maximum C_L ($C_{L,max}$) for K_0 was obtained at 25°, whereas the $C_{L,max}$ angles for the K_1 and K_2 roughness blade profiles were reduced to 22.5°, utilizing the rough surfaces on the suction side. The experimental analysis revealed that the K_2 profile demonstrated a 21% and 19% enhancement in maximal C_L over the K_0 and K_1 profiles, respectively. The highest C_L/C_D was observed with K_1, except at low attack of angle (αoα), where the smooth blade profile resulted in slightly better performance. Experimental analysis showed peak C_L/C_D at αoα of 7.5° for K_0, and 12.5° for both K_1 and K_2, with K_1's optimal C_L/C_D being 2.85% and 8.5% higher than K_0 and K_2, respectively. Numerical analysis indicated that the $C_L/C_{D,avg}$ for K_1 was observed to be 11% and 8% higher than that of K_0 across all αoα.
.

Keywords: *Airfoil; roughness; aerodynamic performance; passive flow control; experimental.*

1. Introduction

The increase in living standards leads to a rise in energy demand. Due to the finite nature of fossil resources and their harmful emissions to the environment, finding alternatives to these resources and more efficient methods of energy production is essential [1-2]. Wind energy is one of these alternative sources. Significant attention has been garnered by wind power within the electricity generation industry due to its easy accessibility and environmental friendly impacts. Hence, enhancements are necessitated for the designs of wind turbines and their components for cost-effective energy conversion. Among these components, a pivotal role in electricity generation is played by the aerodynamic performance of turbine blades, which convert wind energy into mechanical energy. Consequently, the effects of blade design on the aerodynamic performance of wind turbine have been concentrated on by researchers. Researchers have observed stall angles and aerodynamic performances of various symmetrical turbine blade models using both experimental and numerical methods [3-8]. Additionally, the performance of asymmetric blade models, which have become increasingly popular in recent years due to their high efficiency, is also being examined in the literature [9-11].

By employing numerical methods with the k-ε turbulence model, Karthick and Kumar [12] studied the performance coefficients of the NACA 0015 blade profile at αoα ranging from 0 to 20°. Their results were found to concur with those from previous studies on vertical axis wind turbine blades. Rubel et al. [13] experimentally examined the NACA 0015 blade across αoα from 0° to 180°, corroborating their numerical study with experimental outcomes to elucidate how variations in αoα affect the blade's lift coefficients (C_L) and drag coefficients (C_D), and to detail the turbulence, pressure, and velocity distribution around the blade from simulation data. To augment the aerodynamic performance of the NACA 0015 blade profile, the suction side of the trailing edge region was modified with backward steps by Kabir et al. [14], reporting a decrease in C_D attributable to these modifications.

The influence of aspect ratio (AR) on blade aerodynamic performance and stall angle behavior has been documented [15]. The aerodynamic performance of turbine blades at low Reynolds numbers (RE) by altering ARs was experimentally probed by Mizoguchi et al. [16], highlighting that the flow structure at low ARs diverges from that at high ARs at substantial αoα.

To regulate airflow over platforms using blade structures, especially in wind turbines, various flow control methods have been devised. These controls are categorized into active and passive flow control methods. It is marked by the

*Corresponding Author

principal distinction between these flow control strategies that, unlike passive control, which does not require external energy, active control necessitates it. Techniques such as dimples, tubercles [17], vortex generators (including various types of flaps [18-19], wind lenses [20-21], and rough surfaces are widely adopted in the implementation of passive control methods.

In the operational context of wind turbines, the blades are subjected to adverse conditions such as dust, sand, ice, and material deformation, leading to surface roughness. A comprehensive understanding of how surface roughness influences the aerodynamic performance of turbine blades has been necessitated, a topic that has garnered increased focus in recent research efforts. Inspired by the rough regions on the wing surfaces of organisms such as bald eagles and dragonflies, rough areas have been integrated onto the airfoil surface. These applications have begun to be implemented experimentally and are anticipated to be commercialized in the near future [22]. An experimental examination of the aerodynamic consequences of surface roughness on the NACA 0012 profile was undertaken by Chakroun et al. [23], observing a beneficial impact of trailing edge roughness on both the C_L and C_D. In a similar vein, into the effects of micro-scale roughness on blade aerodynamics was delved by Salazar and Barrientos [24], employing angular speckle correlation for roughness assessment and introducing a mathematical formula to quantify uncertainty. The aerodynamic losses attributable to surface roughness were focused on by Zhang et al. [25] through their experimental work, whereas the aerodynamic ramifications of deformations at the leading and trailing edges of blades were explored by Wang et al. [26], proposing a modified NACA 0012 blade profile optimized for vertical axis wind turbines.

Further contributing to this body of work, a numerical analysis on the roughness effects pertinent to blades used in micro air vehicles was conducted by El-Latief et al. [27], comparing the aerodynamic performance of smooth versus roughness blade profiles at ultra-low Reynolds numbers (Re = 1400) and demonstrating a superior C_L for the roughness configuration. Echoing these findings, the superior aerodynamic performance of roughness blade profiles compared to smooth ones at low RE for micro air vehicles was confirmed by Murphy and Hu [28], attributing the enhanced lift to changes in vortex formation and turbulent flow patterns induced by roughness surfaces. The impact of roughness surfaces on turbine blade performance was investigated by Tamai et al. [29], noting that such profiles facilitate an expedited transition from laminar to turbulent flow at low RE, thereby boosting aerodynamic efficiency. Experimental investigations to ascertain how wake turbulence influences blade performance under transonic flow conditions were conducted by Zhang and Ligrani [30]. It was demonstrated that the enhanced flow diffusion region at the suction side of the trailing edge causes wake formation to be significantly influenced by the surface roughness factor. Similarly, the C_L and C_D performances of both smooth and roughness NACA 0012 turbine profiles, utilizing a combination of experimental and numerical methodologies, were assessed by Xia et al. [31]. By varying the angle of attack (αoα), the behaviors of C_L and C_D were documented, noting an improvement in the C_L/C_D for roughness blade profiles at lower αoα compared to smooth profiles.

Liu et al. study on a NACA 23012 revealed that initial ice roughness significantly impacts water film and flow, notably retarding primary wave formation at U_∞=10 m/s and causing rivulets to merge at higher speeds (15 m/s), thus affecting surface water/ice dynamics [32]. Sun et al. proposed a novel multi-objective evolution algorithm to enhance the aerodynamic performance of the NACA2415, mitigating cavitation and surface roughness effects, which resulted in a 20% average increase in the C_L/C_D and a 17.2% average reduction in the minimum peak lift coefficient [33]. Wang et al. study demonstrates that surface roughness, with a magnitude of Ra=157μm, covering 10%, 30%, 50%, and 100% of the suction surface, leads to a respective decrease in profile loss of 14.6%, 16.04%, 16.45%, and 10.20%, highlighting the effective role of surface roughness on aerodynamic performance [34]. Özkan and Erkan's study on the NACA 63-415 airfoil showed that while roughness minimally affected aerodynamics at Re≤104, it significantly enhanced performance between Re of $5\times10_4$ to $1.5\times10_5$, with benefits persisting up to a roughness height of 0.1 mm for Re=$2.5\times10_5$, beyond which roughness reduced the C_L/C_D [35]. Kelly et al. study quantitatively demonstrates that blade roughness on wind turbines decreases performance by 2.9–8.6% and that re-optimizing the controller gain coefficient can enhance annual energy production by 0.1–1.0%, highlighting the potential of control strategies to mitigate roughness effects [36]. Dwivedi et al. experimental study on a NACA 4412 at a RE of $1.7x10^5$ demonstrates how surface roughness, induced at different chord length (c) areas, significantly affects aerodynamic C_L, C_D and stall characteristics, suggesting the potential for controlled roughness application during takeoff and landing to optimize performance [37].

As indicated by the aforementioned studies, surface roughness plays a crucial role and directly impacts the aerodynamic performance of blades. Initial research efforts were predominantly focused on the effects of roughness on the turbine blades of aircraft, such as helicopters and unmanned aerial vehicles. More recently, the emphasis has shifted towards investigating the impact of roughness on wind turbine blades, particularly in the trailing edge region. Nonetheless, the specific effects of roughness situated near the mid-chord region of the blade and its consequent impact on blade performance warrant further exploration. Hence, this study modifies the suction side of the NACA 0015 with single and double roughness regions, respectively, while employing the smooth NACA 0015 profile as a baseline for comparison. Experiments and numerical simulations were conducted at an inlet flow velocity of 10 m/s, corresponding to a RE of 42,800. Results pertaining to C_L, C_D, and the C_L/C_D were compiled. Data derived from numerical analyses were corroborated with experimental findings, which were further substantiated by pressure, velocity, and turbulence intensity contours from the numerical simulations.

2. Experimental Setup and Procedure

2.1 Wind Tunnel Facility

This study's experimental component utilized the HM-170 GUNT model, an open-type wind turbine depicted in Fig. 1. The wind tunnel is segmented into nozzle, test, and diffuser sections. Air is directed through a honeycomb structure in the nozzle section to ensure a uniform flow velocity with minimal turbulence before it accelerates towards the test section. Measurements were conducted exclusively within the test section, characterized by a square cross-section measuring 0.3x0.3 m^2 and extending 0.4 m in length, allowing air to maintain a steady and laminar velocity until it reaches the diffuser section.

At the test section's inlet, pressure parameters and the free-stream velocity (V_∞) are measured using a pitot tube and an inclined manometer, respectively. Based on a wind speed of 10 m/s, experimental and numerical tests were performed by varying the αoα from 0 to 35°, with a Re of 42,800 as the basis. The blade model is centrally mounted in the test section on a metal rod, one end of which connects to a force sensor situated beneath the test section, and the other end affixes to the blade. This setup enables the force sensor to detect two principal force components acting on the blade model: the drag force aligned with the airflow and the lift force acting perpendicular to it.

Given the test section's limited cross-sectional area, a blockage ratio is employed to mitigate the sidewall effects on the blade's flow characteristics. This ratio, which is the blade's surface area relative to the test section's cross-sectional area, is recommended not to exceed 10% [38]. For this study, the blockage ratio was calculated to be 8.9%, obviating the need for any blockage-related corrections.

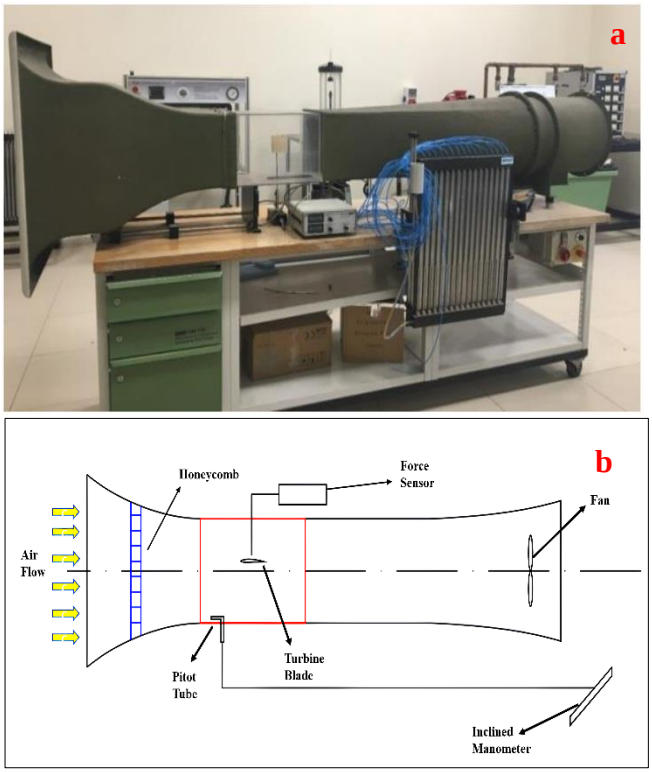

Figure 1. Schematic and Experimental views of Wind tunnel.

2.2 Blade Configurations

To elucidate the impact of roughness surfaces on aerodynamic performance, symmetrical blade models, which are commonly employed in wind turbines and unmanned aircraft, are utilized. This approach enables the identification of how roughness surfaces influence flow separation and reattachment, particularly at a 0°, by comparing the effects on pressure (smooth) and suction (roughness) sides. For this purpose, the study employs a symmetrical NACA (National Advisory Committee for Aeronautics) 0015 four-digit model for experimental investigations. The blade's coordinate data was sourced from the "NACA 4 digit blade generator" [39] as shown in Fig. 2.a Design software was employed to produce three versions of the blade model: a smooth blade model (K_0), a single roughness blade model (K_1), and a double roughness blade model (K_2). Details of the schematic and experimental models are presented in Fig. 3 and Fig. 4, respectively. For all airfoil, the c has been set at 66 mm.

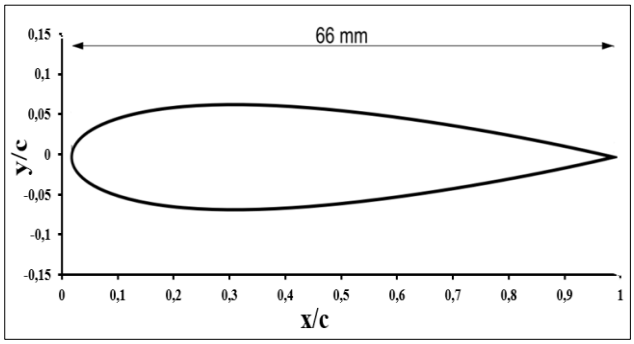

Figure 2. Schematic structure of NACA-0015 turbine blade profile (Smooth blade, K_o).

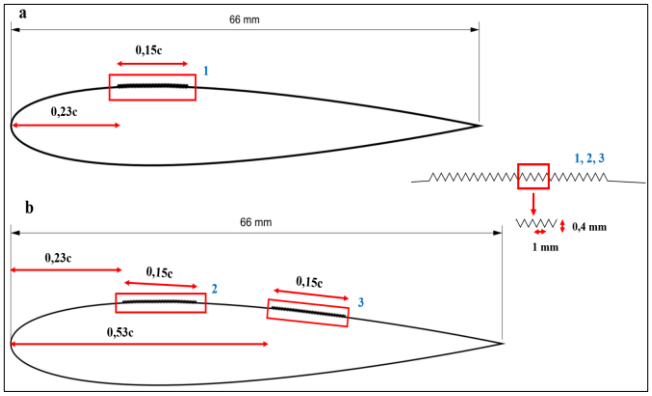

Figure 3. Geometric description of a) K_1 and b) K_2.

In this study, the variation of turbulence and laminar boundary layers in response to an increasing αoα on the blade surface is systematically explored, with an emphasis on the differential impacts of rough versus smooth surface treatments on aerodynamic performance. As depicted in Fig. 3a, a unique roughness configuration (K_1) is engineered on the suction side of the blade, incorporating a spanwise-width roughened area extending 0.15c in length from 0.23c to the leading edge. Given that the onset of turbulent flow begins at the trailing edge, an additional roughness structure is integrated to enhance performance at lower αoαs, resulting in the development of the K_2 profile, as illustrated in Fig. 3b. The initial rough surface is situated 0.23c from the leading edge, while the subsequent one is located 0.53c from the leading edge, with each roughness width uniformly maintained at 0.15c. A primary objective of this study is to delay flow separation on the blade surface by employing surface roughness, aiming to enhance the aerodynamic performance. This model specifically seeks to quantify the influence of surface roughness on blade efficacy within the turbulent boundary layer zone on the suction side.

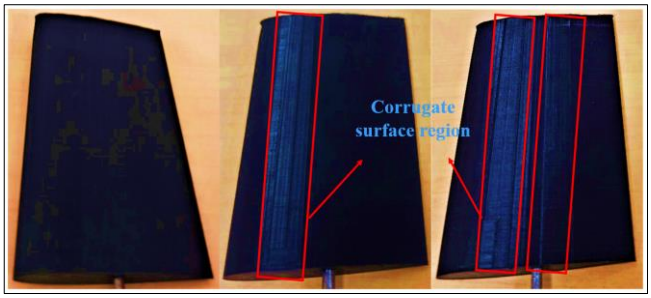

Figure 4. a) Smooth surface b) single and, c) double roughness blade models produced by 3D printer.

The blades utilized in the experimental phase were fabricated using an Ultimaker extended 3D printer. Aerodynamic studies frequently employ a diverse array of materials in the construction of blade models. A primary objective of this study is to minimize surface roughness to accurately capture the blade profile. Consequently, due to its minimal material roughness effect, CPA+ type filament was selected for the production of the blade profile.

To verify the blades' surface roughness quality after the manufacturing process, measurements were conducted using a Mitutoyo J-412 (shown in Fig. 5) 90° / 5 µm Surface Roughness Magnitude (R_a) Tester. The roughness values were assessed at two distinct areas: the blade's smooth surface and the roughness structure. Measurements were taken three times from both the smooth and roughness surfaces of the K_2 model, and their average values were considered for the numerical analysis. According to the sensor's findings, the roughness of the smooth and roughness surfaces was measured to be 1.062 µm and 6.267 µm, respectively.

Table 1. Roughness of the plain and roughness surfaces of the blades model.

Measurement	1.	2.	3.	Measurement_{AVG}
Smooth Surface(µm)	1,061	0,903	1,224	1,062
Roughness Surface(µm)	6,122	6,014	6,665	6,267

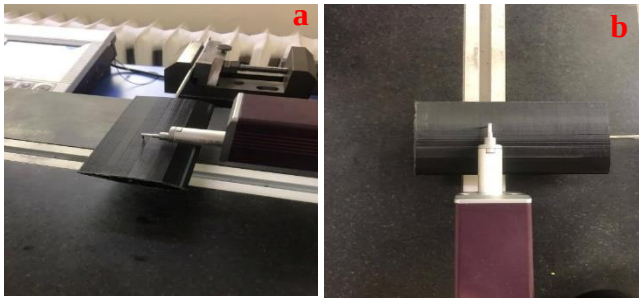

Figure 5. a) Isometric and b) top view of the blades surface during roughness measurements.

There are two non-dimensional coefficients existing for describing the effect of lift and drag forces on the turbine blade profile. Lift coefficient (C_L) and drag coefficient (C_D) are being used to detect the aerodynamic performance of blade [40].

Lift Coefficient:

$$C_L = \frac{2L}{\rho V^2 A} \quad (1)$$

Drag Coefficient:

$$C_D = \frac{2D}{\rho V^2 A} \quad (2)$$

Eq. 3 defines the average aerodynamic performance, which helps in understanding the positive effects of surface roughness on blade performance.

$$C_L/C_{D\,avg} = \frac{\Sigma^{C_L}/_{C_D}}{k} \quad (3)$$

k is the total number of αοα.

2.3 Experimental Uncertainty

Experimental results inherently contain uncertainties, which can be minimized but not completely eliminated. The primary sources of these uncertainties include errors from devices, tools, and materials used during the experiments. The most important factor affecting accuracy is errors that may arise from different reasons during experiments such as error factor of the devices, tools, and materials utilized during the tests. Uncertainties of the devices documented in Table 2, and by using equations 4 and 5 uncertainties for C_L and C_D are calculated and given in Table 3. As seen in Table 3, the obtained uncertainties C_L and C_D are respectively ± 0,036 and ± 0,031. Kline and McClintock methods were used in the uncertainty analysis of the measurement devices used in the experimental study [41]. By using this method, the effect of each variable on the total uncertainty has been taken into account in the expressions in Eq. 5 and 6.

$$R = R(X_1, X_2, X_3, \quad X_N,) \quad (4)$$

$$W_R = \sqrt{\left(\frac{\partial R}{\partial x_1} w_1\right)^2 + \left(\frac{\partial R}{\partial x_2} w_2\right)^2 + \left(\frac{\partial R}{\partial x_3} w_3\right)^2 + \cdots + \left(\frac{\partial R}{\partial x_N} w_N\right)^2} \quad (5)$$

Table 2. Uncertainties for Measuring Instruments.

Measuring device	Uncertainty
Length Measurement (Caliper)	± 2x10^{-5} m
Velocity Measurement (Anemometer)	± 0,10 m/s
Pressure Measurement (Pitot tube)	±0,015 Pa
Force Measurement (Load cell)	± 0,014 N
Roughness surface Measurement (roughness tester)	±0,01 (µm)

Table 3. Maximum uncertainties for calculations.

Calculate	Uncertainty
Lift Coefficient (C_L)	± 0,036
Drag Coefficient (C_D)	± 0,031

3. Numerical Study Setup

3.1 Computational Domain and Mesh

In order to detailedly investigate the flow behavior around the blade models, in the current work, the experiments are supported by numerical simulation. A C-type flow domain is considered to have a cost-effective numerical solution. To reduce the effects of the side boundaries on the blade models, the C-type flow domain is decided to be 36c by 45c, shown in Fig. 6.

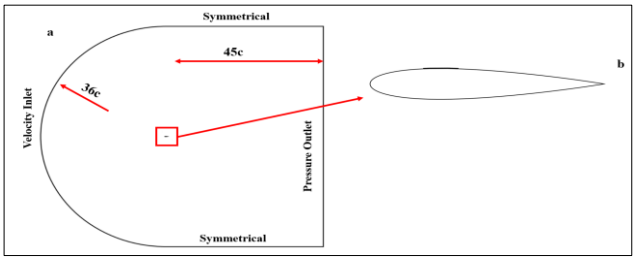

Figure 6. a) C-type domain b) K_1 model.

The curved side of the C-type flow was set with velocity inlet boundary conditions. Therefore, by changing the inlet flow direction, the αοα is adjusted. The inlet flow velocity magnitude is set based on the experimental conditions.

Pressure outlet is used as an exit boundary condition. The numerical solution was performed using Ansys-Fluent.

The mesh was created in the Ansys-Meshing tool by using triangular and rectangular elements. Due to the large velocity and pressure variations in the velocity boundary layer areas on the blade surface, a densified mesh was applied with the edge size command in order to obtain a quality solution. Mesh structure is involved on the Fig. 7a and 7b.

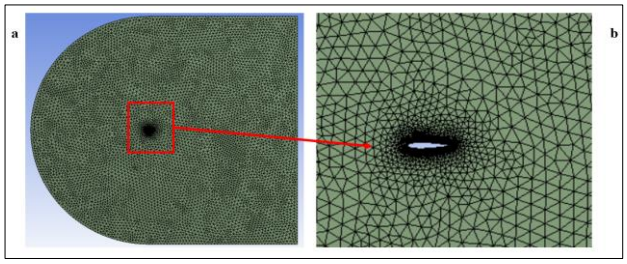

Figure 7. Numerical model mesh: (a) view of the entire domain and (b) close view of the domain.

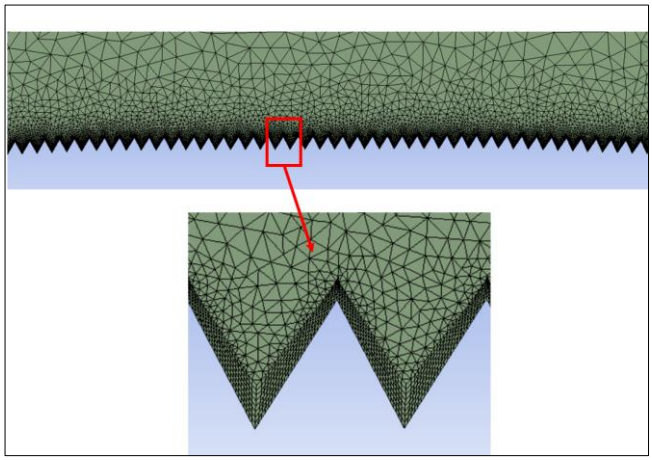

Figure 8. Mesh structure around roughness surface.

To ensure the quality of the numerical solution, mesh independency was applied for K_0 profile. The number elements were increased from 100 946 to 194 978 as seen in Table 4, and solution was obtained at 17.5° αoα. The difference between results around 0.1% is assumed to be good enough; therefore, mesh including 128 986 elements was chosen for smooth blade solution.

Table 4. Independence of Elements amount.

	C_L	C_D	Mesh Elements
Smooth Surface (K_0)	0.9234	0.2848	100946
	0.9311	**0.2859**	**128986**
	0.9320	0.2887	145626
	0.9319	0.2872	153484
	0.9417	0.2871	194978

In addition to mesh independence; mesh quality of the smooth blade is documented based on well-known parameters which are element quality, orthogonal quality and skewness [42]. It is recommended that the values of element quality and orthogonal quality close to 1, while the skewness is close to 0. Also, by considering these qualities of smooth and roughness blades meshes were created and their information is given in Table 5. In addition, Fig. 8 is provided to show details of a mesh around roughness region.

Table 5. Mesh Specifications.

Mesh Quality	Elements	Element Quality	Orthogonal Quality	Skewness
(K_0)	128986	0.9332	0.9332	0.0433
(K_1)	219000	0.9710	0.9710	0.0432
(K_2)	260000	0.9704	0.9704	0.0434

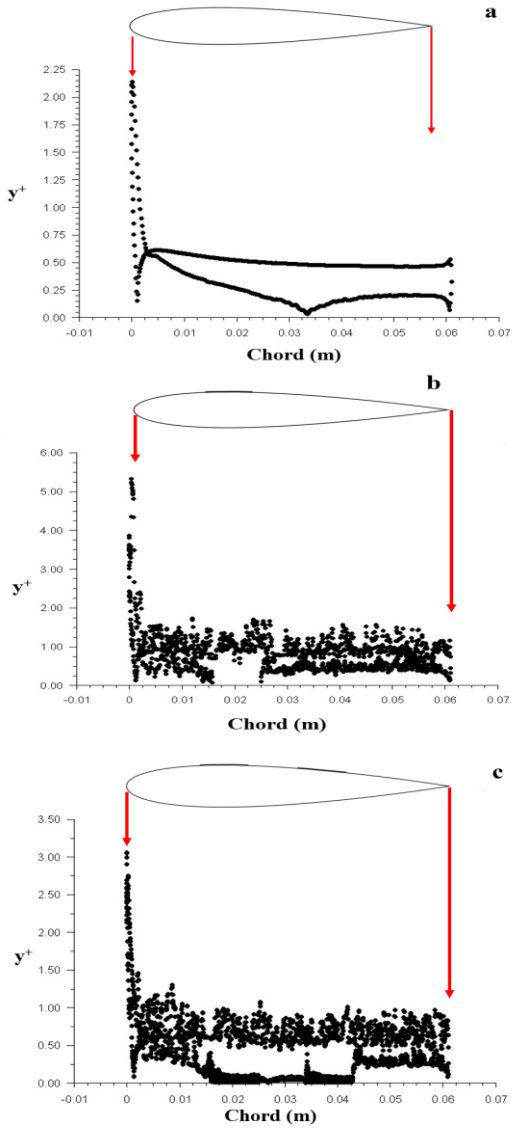

Figure 9. y^+ at 22.5° a) K_0, b)K_1 and c)K_2.

Mesh structure and configuration around the blade are very crucial to achieve a more precise result. y^+ is a nondimensional coefficient and describes thickness of boundary layers [42].

$$y^+ = \frac{U_*.y}{\upsilon} \tag{6}$$

Eq. 6 [43] shows dimensionless y^+ equation, where U* is the friction velocity, y is the distance of the wall and υ is the local kinematic viscosity of the fluid. Boundary layers are divided into 4 regions which are called viscous sub-layer ($y^+ \leq 5$), buffer layer ($5 < y^+ \leq 30$), log-law region ($30 < y^+ \leq 500$) and outer layer [44-45]. In addition to mesh sizes and qualities, to show the credibility of the numerical solutions obtained in the current study, y^+ values where plotted in Fig. 9 for each blade configuration at 17.5° αoα. As seen from the figure, except for the leading edges, y^+ values around or lower than 2 for each configuration; that is boundary layer development on the blade could be captured during the numerical solutions.

In this paper, the numerical simulations are based on incompressible two dimensional steady-state conditions. For the

sake of completeness, the following mass and momentum conservation equations are provided.

$$\frac{\partial \rho}{\partial t} + \rho\, divV = 0 \tag{7}$$

Specific weight of fluid does not change in time [46]

$$\frac{\partial \rho}{\partial t} = 0 \tag{8}$$

Due to specific weight does not change, continuity equation changes into $divV = 0$ or $\nabla . V = 0$ similarly [46].

Conversation of momentum based on the Newton's second law of motion, expresses a proportionality between applied force and the resulting acceleration of a fluid particle.

$$\rho \frac{DV}{Dt} = \rho g + \nabla . \tau_{ij} \tag{9}$$

3.2 Validation of Turbulence Model

In the realm of numerical analyses, the selection of turbulence models is contingent upon the specific domains of application. To ascertain the turbulence model that exhibits the highest fidelity, the C_L versus αoα trends of four distinct turbulence models—Spalart-Allmaras, k-ε realizable, transition SST, and k-ω SST—were juxtaposed with empirical data. Subsequently, the model that demonstrated the closest alignment with the experimental outcomes was identified.

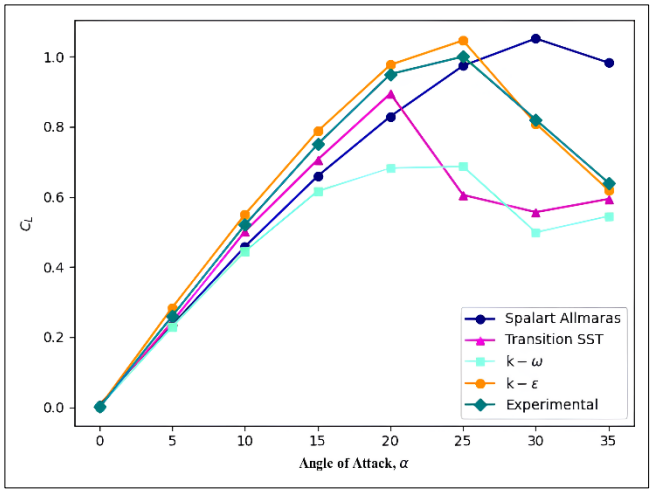

Figure 10. Comparison of C_L values of 4 different turbulence models and experimental study for K_0.

In Fig. 10, the aerodynamic performance of the K_0, as delineated by the C_L versus αoα graph, is juxtaposed against the outcomes derived from various turbulence models. Within the 0 to 5° αoα range, the discrepancies between the C_L values obtained from the experimental investigation and those predicted by the four turbulence models are negligible. However, post-5°, variations in solution accuracy—attributable to turbulence manifesting on the blade surfaces—culminate in discernible deviations among the results yielded by different turbulence models on the graph. Consequently, while the experimental data exhibit variances in comparison to the outcomes of the Spalart-Allmaras and k-ω turbulence models, the Transition SST and k-ε realizable models demonstrate parallel accelerations. With an escalation in αoα, and the ensuing turbulence engendered by vortices over a substantial portion of the blade surface, it was noted that all turbulence models, with the exception of the k-ε realizable model, diverged markedly from the experimental findings. Owing to its congruency in stall angle values and its close alignment with experimental data at elevated αoα, the k-ε realizable model was adjudged the most apt turbulence model for this investigation.

Due to the high compatible with the experimental study, k-ε realizable turbulence model whose equations given in Eq. 10 and Eq. 11 was used to obtain numerical results. Also, k-ε realizable turbulence model has been widely used by researchers [47-48].

For turbulence kinetic energy (k);

$$\frac{\partial}{\partial t}(\rho k) + \frac{\partial}{\partial x_j}(\rho k u_i) = \frac{\partial}{\partial x_j}\left[\left(\mu + \frac{\mu_t}{\sigma_k}\right)\frac{\partial k}{\partial x_j}\right] + G_k + G_b - \rho\epsilon - Y_M + S_k \tag{10}$$

For energy dissipation rate (ε);

$$\frac{\partial}{\partial t}(\rho \epsilon) + \frac{\partial}{\partial x_j}(\rho \epsilon u_i) = \frac{\partial}{\partial x_j}\left[\left(\mu + \frac{\mu_t}{\sigma_\epsilon}\right)\frac{\partial \epsilon}{\partial x_j}\right] + C_1 \frac{\epsilon}{k}(G_k + C_3 G_b) - C_2 \rho \frac{\epsilon^2}{k} + S_\epsilon \tag{11}$$

G_k is described as turbulence kinetic energy due to the velocity and G_b is described as turbulence kinetic energy due to the buoyancy. C is a constant. σ_k *and* σ_ϵ are turbulent Prandtl numbers.

4. Result and Discussions

In this study, to analyze the NACA 0015 and roughness turbine blade profiles aerodynamic performance such as C_L, C_D, C_L /C_D and turbulence kinetic energy, numerical analysis were conducted by using Ansys Fluent Software for between 0-35° each 2.5° degree. This methodical approach allowed for a comprehensive understanding of the aerodynamic behaviors across a broad range of angles, enhancing the reliability of the results.

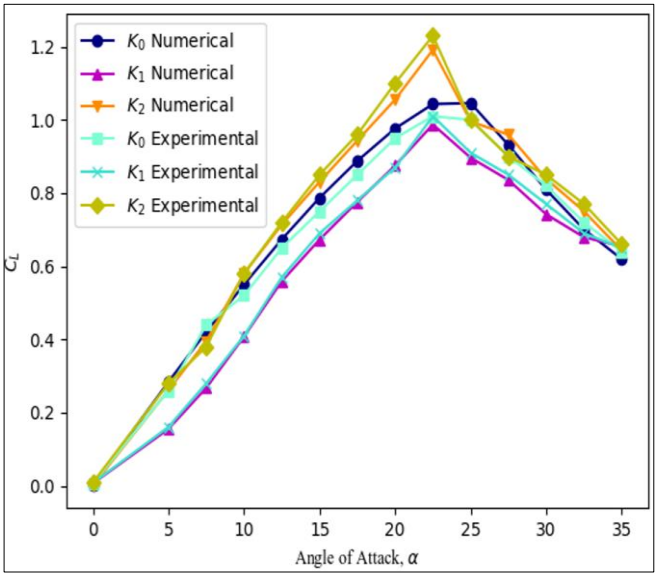

Figure 11. Comparison of C_L values of K_0, K_1 and K_2.

In Fig. 11, the C_L values for the K_0, K_1, and K_2 across the 0-35° αoα range were subjected to both numerical and experimental analysis. Up to a 20° αoα, the behavior of K_0 and K_2 was observed to be analogous. This similarity indicates consistent performance characteristics between

these two models under lower angle conditions. At these αoα, the K_1 blade model exhibited lower C_L values in comparison to its counterparts. The stall angles for the K_1 and K_2 models were identified at 22.5°, whereas the K_0 demonstrated a stall angle at 25. Upon experimental analysis of these metrics, it becomes evident that the maximum C_L performance of the K_2 surpasses that of the K_0 by 19% and the K_1 by 21%. These findings underscore the superior aerodynamic performance of the K_2 model, particularly in post-stall conditions. Both preceding and succeeding the stall point, the K_2 consistently manifested the highest C_L values. At a 35° αoα, the C_L values of the three blade models converge closely. The incorporation of dual roughness structures on the K_2 beyond a 10° αoα, coupled with the emergence of high turbulence density between these structures—as will be elucidated in Fig. 16c—accounts for the superior C_L performance relative to the smooth model. Conversely, the proximal positioning of the roughness structure to the leading edge on the K_1 negates any potential benefits, given that the flow in this region remains laminar at low αoα. Instead, the fluid interaction is confined to the apex of the roughness structure on the blade surface, reducing the contact area and consequently diminishing the drag force in comparison to the other models. Moreover, the restricted flow interaction with the blade's upper surface results in accelerated flow over the smooth blade's upper contour, leading to a reduced pressure differential and thus a lower C_L than that observed in the other two models.

The reason for the lower stall angle is that while rough surfaces increase flow attachment, they also enhance turbulence that can cause earlier flow separation. This is especially true at high αoα, leading to earlier separation of the flow from the airfoil's upper surface and thus, the occurrence of stall at lower angles. This phenomenon underscores the dynamic and complex nature of the impact of rough surfaces on aerodynamic performance.

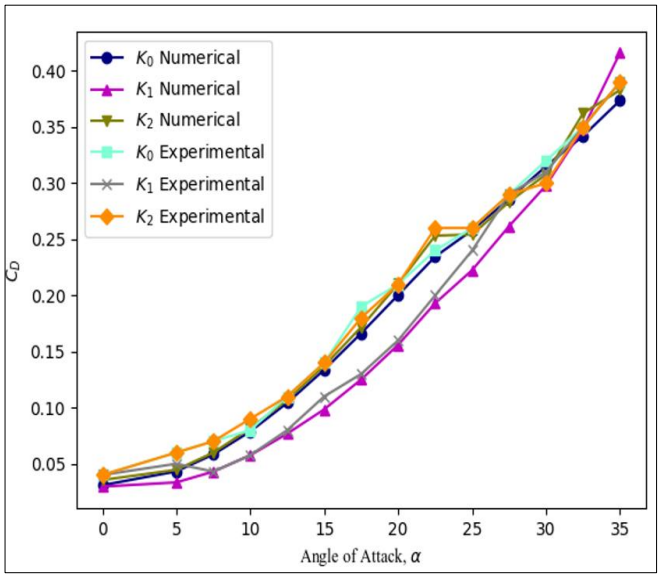

Figure 12. Comparison of C_D values of K_0, K_1 and K_2.

In Fig. 12, the C_D values for the K_0, K_1, and K_2 across the 0-35° αoα range were scrutinized. A negligible variance in C_D was observed among the three blade models within the 0-5° range. In the experimental analysis, it was notably observed that the C_D values for the K_1 were lower than those for the other models from 10-25°. The K_0 and K_2 exhibited analogous behaviors up to a 15° αoα; beyond this point, the K_2 model demonstrated a steeper ascent in C_D up to 22.5° compared to the K_1. It has been determined that at the stall angle of 22.5°, the C_D of K_2 is 10.41% and 38.46% higher compared to K_1 and K_0, respectively.

In the span between 7.5° and 25°, the K_1 manifested the lowest C_D values relative to the other profiles. Notably, a dramatic increase in the C_D for the K_2 occurred between 15° and 25°, with a pronounced decline immediately thereafter. Two distinct types of frictional forces were identified: lift-induced drag, stemming from vortex formation, and parasitic drag, resulting from fluid viscosity. While the diminution of parasitic drag was observable in the other models, it was less apparent in the K_2. This situation suggests that the K2's design might benefit from modifications that specifically address its parasitic drag characteristics. This anomaly can be ascribed to the generation of low-pressure zones between the roughness structures on the K_2's upper surface at a 22° αoα.

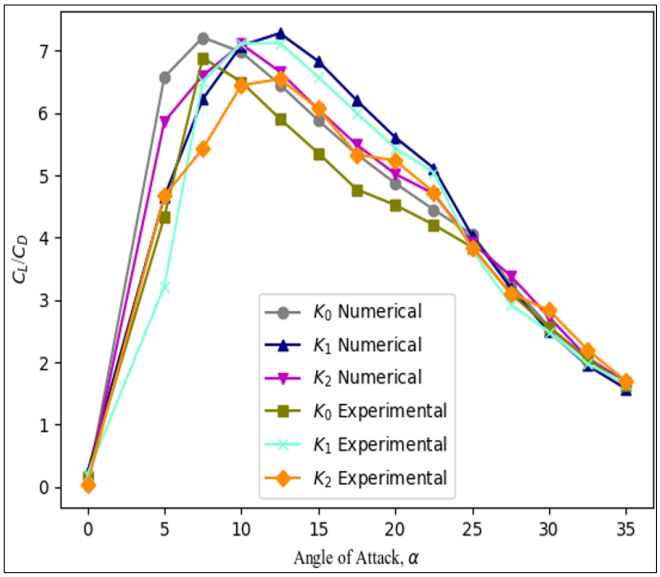

Figure 13. Comparison of C_L / C_D values of K_0, K_1 and K_2 models.

In Fig. 13, the C_L/C_D for the K_0, K_1, and K_2 across the 0-35° αoα range were scrutinized. Within this framework, an expeditious enhancement in C_L/C_D was discerned for all three models from 0 to 5°. In the experimental analysis, it was observed that the K_0, K_1, and K_2 attained their peak C_L/C_D values at 7.5°, 12.5°, and 12.5°, respectively. Upon reaching their apogee of C_L/C_D, it was noted that the K_1 model's value surpassed that of K_0 and K_2 by 2.85% and 8.5%, respectively. Subsequent to the models achieving their maximal αoα, a linear decrement in aerodynamic efficiency was observed, attributable to the swift escalation of C_D values. Between 10-25° αoα, the C_L/C_D of K_1 markedly outperformed the other two models, with the smooth blade exhibiting the lowest efficacy within these angular intervals. As previously elucidated in Fig. 12, K_1's superior performance within these αoα ranges compared to the other models is attributed to its significantly lower C_D values.

The average aerodynamic efficiency, denoted as $C_L/C_{D,avg}$, represents the quotient of C_L/C_D values spanning the 10 to 25° interval, wherein these values were assessed. Utilizing Eq. 3, numerical analysis calculated the comparative $C_L/C_{D,avg}$ of K_1 to be 11% and 8% higher than that of K_0 and K_2, respectively. Although the three models exhibited proximate values in the 25-35° range, K_2

demonstrated marginally superior performance. An overarching analysis of Fig. 13 revealed that the roughness structure exerts a beneficial impact on both the maximal and $C_L/C_{D,avg}$.

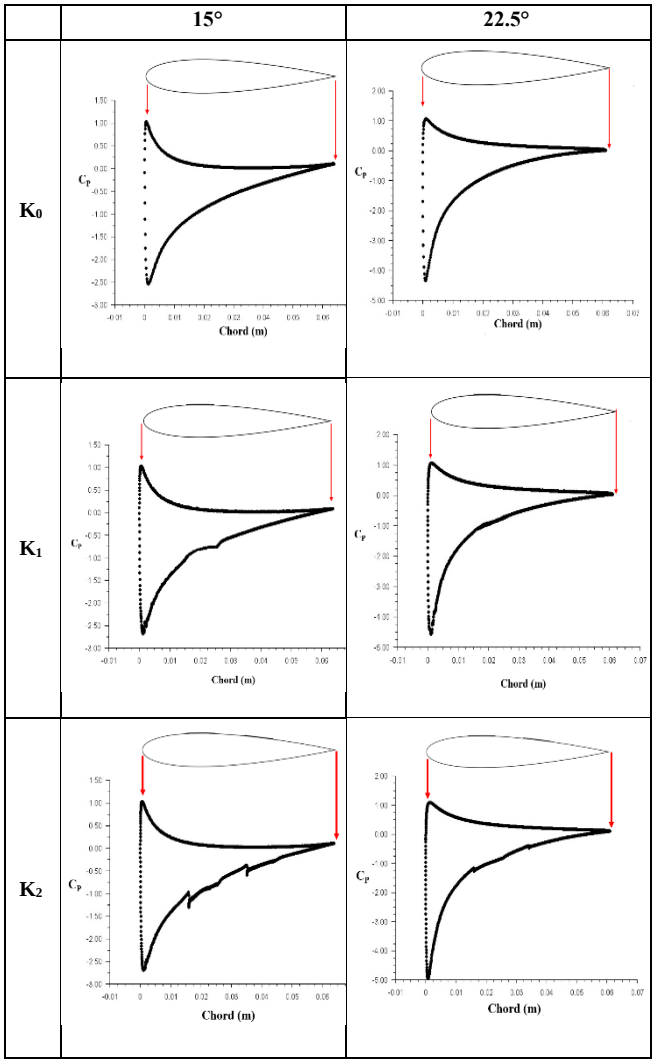

Figure 14. C_P for three turbine blade profiles at 15° and 22,5° αoα.

Fig. 14 illustrates the pressure coefficient (C_P) across the c of the K_0, K_1, and K_2 at both 15° and 22.5° αoα. For all blade models, a pronounced pressure differential was evident in the leading-edge region at both αoα. At 15°, a substantial pressure disparity spanned from the leading edge to the trailing edge on the upper surface of the blades, whereas at 22.5°, the magnitude of this pressure variation was significantly reduced. This reduction in pressure disparity at 22.5° facilitated the emergence of turbulence in the upper region of the blade surfaces, attributable to vortex generation. Consequently, the pressure attained a distinctively lower minimum level, as the flow was not sustained over a considerable portion of the blade surface. Upon meticulous examination of the K_2, it was discerned that the C_P in the vicinity of the roughness structure's commencement exhibited a disparate acceleration in comparison to the K_0. The roughness structure engendered lower pressure zones within this blade region, thereby enhancing the generation of a higher C_L.

In Fig. 15, the pressure contours and streamline configurations for the K_0, K_1, and K_2 at 15°, 22.5°, and 35° are depicted. In the K_0 model, a linear increase in vortex formation from the trailing edge towards the leading edge is noted, attributable to the escalation in the αoα. This pattern of vortex formation is a key indicator of how the blade surfaces interact with the flow field, particularly in terms of energy transfer and boundary layer behavior. Conversely, in the K_1 and K_2 models, vortex zones are identified in vicinities where the roughness structures terminate. While the upper surface of the flat airfoil model predominantly exhibits laminar flow, the introduction of roughness structures in the K_1 and K_2 culminates in regions of heightened turbulence.

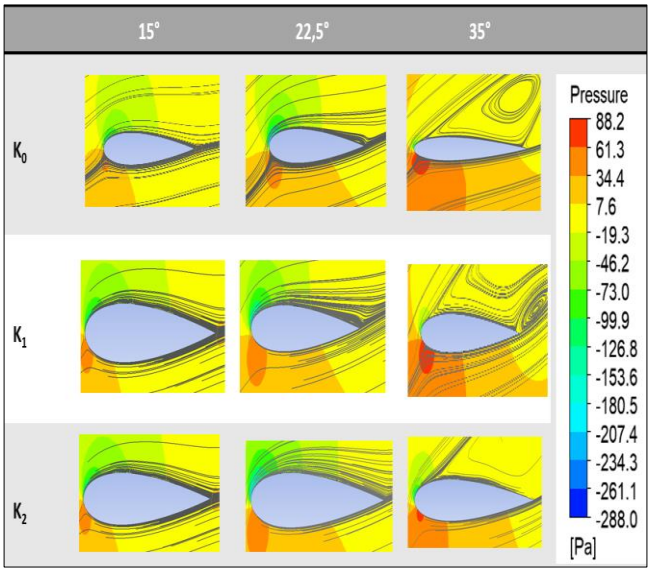

Figure 15. Pressure contours and streamlines of blade profiles at 15 °, 22.5 ° and 35 °, respectively a) K_0 b) K_1 and, c) K_2.

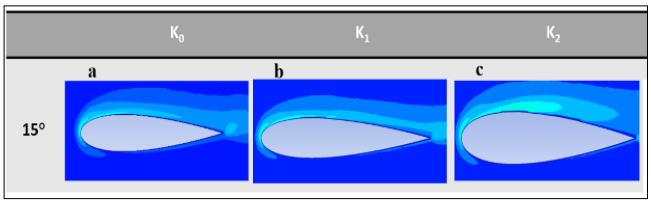

Figure 16. Turbulence kinetic energy of blade profiles at 15°, 22.5° and 35°, respectively a) K_0 b) K_1 and, c) K_2.

Fig. 16 presents the turbulence kinetic energy distribution profiles for K_0, K_1, and K_2 at a 15° αoα. Flow separation on the blade surface engenders turbulence, with turbulence kinetic energy serving as a pivotal indicator of the initiation point, magnitude, and directional trajectory of the turbulent zone. For the K_0, an intensification of turbulence kinetic energy is observed as the flow progresses towards the trailing edge at a 15° αoα. However, in the K_1 and K_2 models, wake regions emerge at both the mid and trailing edges of the turbine blade profiles, a consequence of the roughness surfaces. The emergence of these wake regions is a direct result of how the roughness modifies the flow, emphasizing the importance of surface roughness in controlling flow separation. As unequivocally demonstrated in Fig. 16c, the K_2 model exhibits a substantially higher turbulence density on the upper side of the blade relative to the other models, aligning with the C_L & αoα graph in Fig. 11, where the K_2 is attributed with the peak C_L value at 15°.

In summation, while the K_0 reveals turbulence intensity propagation from the trailing edge towards the leading edge across its surface pre-stall, the K_1 and K_2 not only exhibit turbulence density migration from the trailing to the leading edge but also within and between the roughness structures at

the blade's posterior regions. This configuration results in superior C_L/C_D for the K_1 and K_2 in the pre-stall phase. Post-stall, however, the aerodynamic efficiency contributions of the roughness structures are observed to be constrained.

The results of this study demonstrate that the effects of rough surfaces on aerodynamic performance extend beyond simply enhancing flow attachment. They also offer a deep understanding of how these effects can alter the aerodynamic characteristics of a airfoil, particularly the stall angle. These findings provide significant insights into how the use of rough surfaces in aerodynamic design can be optimized not just for maximizing the aerodynamic advantages of a specific surface but also for improving the overall aerodynamic performance of the airfoil. In this study, the positive effects of surface roughness on aerodynamic performance have been substantiated, particularly through its influence on the coefficient of pressure.

5. Conclusion

In this investigation, NACA 0015 turbine blade profiles with varying rough surfaces, alongside a smooth surface, were scrutinized for their aerodynamic performance, encompassing the lift-to-drag ratio (C_L/C_D), lift coefficient (C_L), drag coefficient (C_D), and turbulence kinetic energy. The gathered data from this study, incorporating both numerical outcomes from Ansys Fluent and experimental findings, were juxtaposed for analysis. The ensuing conclusions can be drawn from this investigation:

- The amalgamation of experimental and numerical analyses substantiates that the implementation of passive flow control methodologies exerts a favorable influence on the aerodynamic efficiency of the airfoil.
- CFD analyses employing diverse turbulence models revealed closely aligned results at lower αoα, with disparities emerging due to increases in αoα. This variation stems from the flow's transition to irregularity, where different turbulence models offer divergent approaches to resolving the phenomenon.
- The onset of stall was pinpointed at a 25° αoα for the K_0 within the analytical framework. Additionally, stalls were precipitated at a 22.5° αoα for the K_1 and K_2. A congruence in stall angle values was observed when experimental studies were aligned with analytical results.
- In the experimental analysis, relative to the maximal C_L values, the K_2 profile exhibited a 21% and 19% enhancement over the K_0 and K_1 profiles, respectively. Post-stall, the K_2 demonstrated a notably higher C_L performance compared to the other models, as confirmed through experimental and numerical methods.
- Between 10-25° αoα, K_1 showed a more advantageous C_D performance than both K_0 and K_2, a finding substantiated by numerical analysis, particularly at higher αoα. At the stall angle of 22.5°, it has been established that the C_D value for K_2 exceeds those of K_1 and K_0 by 10.41% and 38.46%, respectively.
- The peak C_L/C_D values were recorded at αoα of 7.5° for K_0, 12.5° for K_1, and 12.5° for K_2, with K_1 showing 2.85% and 8.5% higher optimal C_L/C_D ratios than K_0 and K_2, respectively, as determined through numerical analysis.
- According to numerical analysis, the $C_L/C_{D,avg}$ for K_1 was found to be 11% and 8% higher than that of K_0 across all αoα, highlighting K_1's enhanced aerodynamic efficiency through the use of numerical methods.

The results of this study demonstrate that the effects of rough surfaces on aerodynamic performance extend beyond simply enhancing flow attachment. They also offer a deep understanding of how these effects can alter the aerodynamic characteristics of a airfoil, particularly the stall angle. These findings provide significant insights into how the use of rough surfaces in aerodynamic design can be optimized not just for maximizing the aerodynamic advantages of a specific surface but also for improving the overall aerodynamic performance of the airfoil.

Author contribution statements

In the scope of this study, Himmet Erdi TANÜRÜN has made contribution to the concepts of literature review, research planning, design and direction of experimental studies, evaluation of results, supply of resources and materials, and writing of the article.

In the scope of this study, Ahmet Giray AKIN has made contribution to the concepts of literature review, research planning, design and direction of experimental studies, supply of resources and materials, and writing of the article.

In the scope of this study, Adem ACIR has made contribution to design and direction of experimental studies, research planning, and evaluation of results.

In the scope of this study, İzzet ŞAHİN has made contribution to control of spelling, creation of graphics and tables from the results of experiments and writing of the article.

Acknowledgements:

Experimental part of this study was carried out in the wind tunnel facility at Gazi University Technology Faculty Energy Systems Engineering Department.

Nomenclature

AR	Aspect Ratio	-
C_l	Lift Coefficient	-
C_d	Drag Coefficient	-
C_l/C_d	Aerodynamic Efficiency	-
Re	Reynolds Numbers	-
C_P	Pressure Coefficient	-
$C_L/C_{D,avg}$	Average Aerodynamic Efficiency	-
c	Chord Length	m
V_∞	Free-Stream Velocity	m/sn
y^+	Thickness of Boundary Layers	m
y	The Distance of the Wall	m
k	Turbulence Kinetic Energy	m^2/s^2
A	Surface Area	m^2
R_a	Surface Roughness Magnitude	μm

Greek Symbols

αoα	Angle of Attack	degree
ε	Energy Dissipation Rate	m^2/s^3
G_k	Turbulence kinetic energy due to the Velocity	m^2/s^2
G_b	Buoyancy Kinetic Energy due to the Velocity	m^2/s^2
σ_k and σ_ϵ	Turbulent Prandtl Numbers	-
υ	Local Kinematic Viscosity of the Fluid	m^2/s
k	Turbulence Kinetic Energy	m^2/s^2
U*	Friction Velocity	m/sn

Abbreviations

K_0	Smooth Blade
K_1	Single Roughness Blade
K_2	Double Roughness Blade

References:

[1] A. Dağdeviren, E. Gedik, A. Keçebaş, H. K. Pazarlıoğlu, K. Arslan, A. I. Alsabery, "Effect of Al2O3–SiO2/Water Hybrid Nanofluid Filled in a Square Enclosure on the Natural Convective Heat Transfer Characteristics: A Numerical Study," *Journal of Nanofluids*, 11(5), 772-781, 2022, doi: 10.1166/jon.2022.1881.

[2] H. E. Tanürün, İ. Ata, M. E. Canli, A. Acir, " Farklı Açıklık Oranlarındaki NACA-0018 Rüzgâr Türbini Kanat Modeli Performansının Sayısal ve Deneysel İncelenmesi," *Politeknik Dergisi*, 23(2), 31-381, 2020 doi:10.2339/politeknik.500043.

[3] M. H. Mohamed, "Performance investigation of H-rotor Darrieus turbine with new airfoil shapes," *Energy*, 47(1), 522-530, 2012, doi: 10.1016/j.energy.2012.08.044.

[4] İ. Şahin, A. Acir, "Numerical and experimental investigations of lift and drag performances of NACA 0015 wind turbine airfoil," *International Journal of Materials, Mechanics and Manufacturing*, 3(1), 22-25, 2015.

[5] N. M. Triet, N. N. Viet, P. M. Thang, "Aerodynamic analysis of aircraft wing," *VNU Journal of Science: Mathematics-Physics*, 31(2), 68-75, 2015.

[6] R. I. Rubel, M. K. Uddin, M. Z. Islam, M. Rokunuzzaman, "Comparison of Aerodynamics Characteristics of NACA 0015 & NACA 4415," *International Journal of Research – Granthaalayah*, 5(11), 187-197, 2016, doi: 10.20944/preprints201610.0095.v1.

[7] A. Ramadan, K. Yousef, M. Said, M. H. Mohamed, "Shape optimization and experimental validation of a drag vertical axis wind turbine," *Energy*, 151, 839-853, 2018, doi: 10.1016/j.energy.2018.03.117.

[8] H. E. Tanürün, A. G. Akın, A. Acır, "Rüzgâr türbinlerinde kiriş yapısının performansa etkisinin sayısal olarak incelenmesi," *Politeknik Dergisi*, 24(3), 1219-1226, 2021. doi: 10.2339/politeknik.845804.

[9] R. Çakıroğlu, H. E. Tanürün, A. Acır, F. Üçgül, S. Olkun, "Optimization of NACA 4412 augmented with a gurney flap by using grey relational analysis," *Journal of the Brazilian Society of Mechanical Sciences and Engineering*, 45(3), 167, 2023. doi: 10.1007/s40430-023-04089-x.

[10] M. M. M. Saad, S. B. Mohd, M. F. Zulkafli, W. M. E. Shibani, "Numerical analysis for comparison of aerodynamic characteristics of six airfoils," *AIP Conference Proceedings*, 1831, 020004, 2017, doi: 10.1063/1.4981145.

[11] V. Shukla, A. K. Kaviti, "Performance evaluation of profile modifications on straight-bladed vertical axis wind turbine by energy and Spalart Allmaras models," *Energy*, 126, 766-795, 2017, doi: 10.1016/j.energy.2017.03.071.

[12] M. Karthick, S. M. Kumar, "Investigation of Aerodynamic Performances of NACA 0015 Wind Turbine Airfoil," *International Journal of Engineering Research*, 5(4), 327-331, 2016, doi: 10.17950/ijer/v5s4/425.

[13] R. I. Rubel, M. K. Uddin, M. Z. Islam, M. D. Rokunuzzaman, "Numerical and experimental investigation of aerodynamics characteristics of NACA 0015 aerofoil," *International Journal of Engineering Technologies*, 2(4), 132-141, 2016, doi: 10.19072/ijet.280499.

[14] A. Kabir, M. S. Chowdhury, M. J. Islam, M. Islam, "Numerical Assessment of the Backward Facing Step for NACA 0015 Airfoil using Computational Fluid Dynamics," *1st International Conference on Advances in Science, Engineering and Robotics Technology (ICASERT*), Bangladesh, May. 3-5, 2019, doi: 10.1109/ICASERT.2019.8934501.

[15] L. W. Traub, "Aerodynamic impact of aspect ratio at low Reynolds number," *Journal of Aircraft*, 50(2), 626-634, 2013. doi: 10.2514/1.C031980.

[16] M. Mizoguchi, Y. Kajikawa, H. Itoh, "Aerodynamic characteristics of low-aspect-ratio wings with various aspect ratios in low Reynolds number flows," *Transactions of The Japan Society for Aeronautical and Space Sciences*, 59(2), 56-63, 2016, doi: 10.2322/tjsass.59.56.

[17] H. E. Tanürün, A. Acir, "Modifiye edilmiş NACA-0015 kanat yapısında tüberkül etkisinin sayısal analizi," *Politeknik Dergisi*, 22(1), 185-195, 2019, doi: 10.2339/politeknik.391800.

[18] M. T. Javaid, U. Sajjad, S. S. ul Hassan, S. Nasir, M. U. Shahid, A. Ali, S. Salamat, "Power enhancement of vertical axis wind turbine using optimum trapped vortex cavity," *Energy*, 278, 127808, 2023, doi: 10.1016/j.energy.2023.127808.

[19] H. E. Tanürün, "Improvement of vertical axis wind turbine performance by using the optimized adaptive flap by the Taguchi method," *Energy Sources, Part A: Recovery, Utilization, and Environmental Effects*, 46(1), 71-90, 2024, doi: 10.1080/15567036.2023.2279264.

[20] I. Hashem, M. H. Mohamed, "Aerodynamic performance enhancements of H-rotor Darrieus wind turbine," *Energy*, 142, 531-545, 2018, doi: 10.1016/j.energy.2017.10.036.

[21] H. E. Tanürün, A. Acır, "Investigation of the hydrogen production potential of the H-Darrieus turbines combined with various wind-lens," *International Journal of Hydrogen Energy*, 47(55), 23118-23138, 2022, doi: 10.1016/j.ijhydene.2022.04.196.

[22] K. Malik, M. Aldheeb, W. Asrar, S. Erwin, "Effects of bio-inspired surface roughness on a swept back tapered NACA 4412 wing," *Journal of Aerospace Technology and Management*, 11, 1719, 2015, doi: 10.5028/jatm.v11.1021.

[23] W. Chakroun, I. Al-Mesri, S. Al-Fahad, "Effect of surface roughness on the aerodynamic characteristics of a symmetrical airfoil," *Wind Engineering*, 28(5), 547-564, 2004, doi: 10.1260/0309524043028136.

[24] F. Salazar and A. Barrientos, "Surface roughness measurement on a wing aircraft by speckle correlation," *Sensors*, 13(9), 11772-11781, 2013, doi: 10.3390/s130911772.

[25] Q. Zhang, M. Goodro, P. M. Ligrani, R. Trindade, S. Sreekanth, "Influence of surface roughness on the aerodynamic losses of a turbine vane," *ASME J. Turbomach*, 128, 568–578, 2006, doi: 10.1115/1.2175163.

[26] Y. Wang, H. Tong, H. Sima, J. Wang, J. Sun, D. Huang, "Experimental study on aerodynamic performance of deformable blade for vertical axis wind turbine," *Energy*, 181, 187-201, 2019, doi: 10.1016/j.energy.2019.03.181.

[27] M. E. Abdel-Latief, K. Elsayed, M. Madbouli Abdelrahman, "Aerodynamic study of the corrugated airfoil at ultra-low Reynolds number," *Advances in Mechanical Engineering*, 11(10), 1-15, 2019, doi: 10.1177/1687814019884164.

[28] J. T. Murphy and H. Hu, "An experimental study of a bio-inspired corrugated airfoil for micro air vehicle applications," *Experiments in fluids*, 49(2), 531-546, 2010, doi: 10.1007/s00348-010-0826-z.

[29] M. Tamai, Z. Wang, G. Rajagopalan, H. Hu, G. He, "Aerodynamic performance of a corrugated dragonfly airfoil compared with smooth airfoils at low Reynolds numbers," *45th AIAA aerospace sciences meeting and exhibit*, Jan. 8-11 2007, Reno, USA, doi: 10.2514/6.2007-483.

[30] Q. Zhang and P. M. Ligrani, "Wake turbulence structure downstream of a cambered airfoil in transonic flow: effects of surface roughness and freestream turbulence intensity," *International Journal of Rotating Machinery*, 8, 1-12, 2006, doi: 10.1155/IJRM/2006/60234.

[31] Y. Xia, O. Bilgen, M. I. Friswell, "The effect of corrugated skins on aerodynamic performance," *Journal of Intelligent Material Systems and Structures*, 25(7), 786-794, 2014, doi: 10.1177/1045389X14521874

[32] Liu, Y., Zhang, K., Tian, W., Hu, H., "An experimental study to characterize the effects of initial ice roughness on the wind-driven water runback over an airfoil surface," *International Journal of Multiphase Flow*, 126, 103254, 2020, doi: 10.1016/j.ijmultiphaseflow.2020.103254

[33] Sun, Z., Mao, Y., Fan, M., "Performance optimization and investigation of flow phenomena on tidal turbine blade airfoil considering cavitation and roughness," *Applied Ocean Research*, 106, 102463, 2021, doi: 10.1016/j.apor.2020.102463.

[34] M. Wang, C. Yang, Z. Li, S. Zhao, Y. Zhang, X. Lu, "Effects of surface roughness on the aerodynamic performance of a high subsonic compressor airfoil at low Reynolds number," *Chinese Journal of Aeronautics*, 34(3), 71-81, 2021, doi: 10.1016/j.cja.2020.08.020.

[35] M. Özkan, O. Erkan, "Control of a boundary layer over a wind turbine blade using distributed passive roughness," *Renewable Energy*, 184, 421-429, 2022, doi: 10.1016/j.renene.2021.11.082.

[36] J. Kelly, C. Vogel, R. Willden, "Impact and mitigation of blade surface roughness effects on wind turbine performance," *Wind Energy*, 25(4), 660-677, 2022, doi: 10.1002/we.2691.

[37] Y. D. Dwivedi, A. Wahab, A. D. Pallay, A. Shesham, "Effect of surface roughness on aerodynamic performance of the wing with NACA 4412 airfoil at Reynolds number 1.7× 105," *Materials Today: Proceedings*, 56, 468-476, 2022, doi: 10.1016/j.matpr.2022.02.153.

[38] J. Ryi, W. Rhee, U. C. Hwang, J. S. Choi, "Blockage effect correction for a scaled wind turbine rotor by using wind tunnel test data," *Renewable Energy*, 79, 227-235, 2015, doi: 10.1016/j.renene.2014.11.057.

[39] A. Tools, "NACA 4-digit airfoil generator," National Advisory Committee for Aeronautics, 2015. http://airfoiltools.com/airfoil/naca4digit (accessed July. 11, 2024).

[40] J. Yao, W. Yuan, J. Xie, H. Zhou, M. Peng, Y. Sun, "Numerical simulation of aerodynamic performance for two dimensional wind turbine airfoils," *Procedia Engineering*, 31, 80-86, 2012, doi: 10.1016/j.proeng.2012.01.994.

[41] S. J. Kline, F. A. McClintock, Describing uncertainties in single-sample experiments, *Mechanical Engineering* 75, 3–8, 1953.

[42] J. Anderson, Computational Fluid Dynamics: The Basics with Applications. McGraw-Hill Education, 1995.",

[43] H. E. Tanürün, "Taguchi Yöntemiyle Sağlamlık Oranının Dikey Eksenli Rüzgâr Türbini Performansına Olan Etkisinin Sayısal Olarak İncelenmesi," *Journal of Materials and Mechatronics: A*, 4(2), 355-372, 2023, doi: 10.55546/jmm.1295748.

[44] M. Tahani, N. Babayan, S. Mehrnia, M. Shadmehri, "A novel heuristic method for optimization of straight blade vertical axis wind turbine," *Energy Conversion and Management*, 127, 461-476, 2016, doi: 10.1016/j.enconman.2016.08.094.

[45] H. F. Lam, H. Y. Peng, "Study of wake characteristics of a vertical axis wind turbine by two-and three-dimensional computational fluid dynamics simulations," *Renewable Energy*, 90, 386-398, 2016, doi: 10.1016/j.renene.2016.01.011.

[46] R. H. Rogers, Fluid Mechanics. Tata McGraw Hill Education Private, 1978.",

[47] M. H. Mohamed, A. M. Ali, A. A. Hafiz, "CFD analysis for H-rotor Darrieus turbine as a low speed wind energy converter," *Engineering Science and Technology, an International Journal*, 18(1), 1-13, 2015, doi: 10.1016/j.jestch.2014.08.002.

[48] A. F. Kaya, H. E. Tanürün, A. Acır, "Numerical investigation of radius dependent solidity effect on H-type vertical axis wind turbines," *Politeknik Dergisi*, 25(3), 1007-1019, 2021, doi: 10.2339/politeknik.799767.